energies

MDPI

Article

A Modified Self-Synchronized Synchronverter in Unbalanced Power Grids with Balanced Currents and Restrained Power Ripples

Xiaohe Wang [1], Liang Chen [1], Dan Sun [1,*], Li Zhang [2] and Heng Nian [1]

[1] College of Electrical Engineering, Zhejiang University, Hangzhou 310027, China; 21410053@zju.edu.cn (X.W.); 21410077@zju.edu.cn (L.C.); nianheng@zju.edu.cn (H.N.)

[2] State Key Laboratory of Operation and Control of Renewable Energy & Storage Systems, China Electric Power Research Institute, Beijing 100192, China; zhangli82@epri.sgcc.com.cn

* Correspondence: sundan@zju.edu.cn; Tel.: +86-1368-578-8025

Received: 31 January 2019; Accepted: 6 March 2019; Published: 10 March 2019

Abstract: This paper proposes a modified self-synchronized synchronverter for unbalanced power grids. Small signal analysis of the conventional synchronverter shows that its stability margin around 50 Hz is very limited. Thus, power ripples will be caused at the frequency of 50 Hz. Filter- based current feeding loops are adopted in the conventional synchronverter in order to enhance its stability and eliminate power ripples. In addition, the characteristics of the conventional synchronverter in unbalanced power grids are analyzed, and an improved strategy using a resonant controller is proposed to restrain the current harmonics and power ripples. The parameter design is also studied for the proposed synchronverter. Experimental studies prove that the proposed strategy can achieve precise self-synchronization when the grid voltage is unbalanced, and the power-control performance is also improved significantly.

Keywords: synchronverter; power ripple elimination; resonant controller; unbalanced power grid

1. Introduction

With the rapid development of renewable power generation technologies such as wind power and photovoltaic, distributed generation system has become an effective way to meet load growth, reduce environmental pollution, and improve energy efficiency. DC/AC converters are one of the most common interfaces between the distributed generation system and the power grid. Traditional vector control strategies of DC/AC converters mainly aim to achieve a fast dynamic response [1]. Moreover, the power control of renewable energy is often set as maximum power point tracking (MPPT) in order to harvest as much energy as possible [2,3]. However, compared with the synchronous generators (SG), the DC/AC converters controlled by these strategies have no inertia, and they cannot provide frequency support for the power grid [4,5].

In order to achieve grid-friendly control performance similar as the SG, virtual synchronous generator (VSG) strategies are proposed [6]. The active power control loop of VSG is designed based on the swing equations, and the reactive power control loop is similar as the droop control strategy. In addition, the renewable power generation system should work with enough margins to support the grid, or the energy storage devices are needed to provide the extra active power. Therefore, the inertia property of SG can be inherited by the VSG [7,8]. In most of the VSG strategies, the phase-locked loop (PLL) is needed to detect the phase angle of grid voltages in order to synchronize with the grid [9], or to provide grid frequency information [10]. The PLL is a nonlinear control block which may complicate the system analysis. Therefore, some PLL excluded VSG strategies are proposed [11,12],

where the converter can be synchronized with grid voltage by power balance of swing equations instead of tracking the phase angle of grid voltage directly by PLL. Among these VSG strategies, the synchronverter proposed in [13,14] can emulate the model of SG more accurately. Its reactive power control loop is designed based on the excitation control of SG rather than the droop control. Therefore, the synchronverter makes the renewable power generation system interfaced with the grid like conventional SG and have been paid much attention [15].

The works analyzed above all focus on synchronverters in balanced three-phase systems. However, since the distributed renewable power generation system is usually installed in remote or offshore areas, the grid faults cannot be avoided. Therefore, the performance of synchronverter needs to be investigated under both normal and non-ideal grid conditions. Single-phase voltage drop is one kind of common grid faults which will result in unbalanced power grids [16]. When the grid voltage becomes unbalanced, the negative sequence grid voltage will cause negative sequence grid currents and double frequency power ripples, which severely deteriorate the performance of the converter [17]. However, there is no literature focused on the modification of synchronverter in unbalanced power grids. Resonant controllers have been widely adopted in the improved control strategies under unbalanced power grid conditions to deal with the negative sequence components and proven to be an effective way to deal with this problem. Different kinds of resonant controllers are combined with the vector control (VC) and direct power control (DPC), i.e., second-order generalized integrator (SOGI) [18] reduced-order generalized integrator (ROGI) [19] and reduced-order vector integrator (ROVI) [20]. Theoretical analyses and experimental studies have verified the effectiveness of the resonant based strategies in unbalanced power grid. However, no research has been made to investigate the validity of resonant controller in synchronverter in unbalanced power grid. This is one of the motivations of this study.

Though being a grid-friendly converter, the stability of the synchronverter should be re-evaluated because there is a considerable parameter inconsistence between the synchronverter and physical conventional SG [21]. The stability analysis and control parameter tuning of the synchronverter are not easy due to its characteristics of more complicated nonlinearity. Global stability of the synchronverter was investigated in [22]. However, the stability analysis of the synchronverter in an unbalanced power grid, as well as the impact of the modified controller to the stability of the synchronverter, will be more complicated, and has not been examined yet. The linearization method has been widely adopted to analyze synchronverter systems. In [23], a small-signal sequence impedance model was established to compare the characteristics between VSG and the traditional strategy for grid-connected inverters. In [24], small signal model of synchronverter is established to analyze the stability of the battery system. The small signal models are also established in [25,26] to design the parameters of synchronverter in order to achieve better dynamic performance. It can be seen that the small signal model can reflect the stability of the system at specific steady operation point in a wide frequency range. Therefore, it is meaningful to establish the small signal model for synchronverter in both balanced and unbalanced power grid to study its stability performance and design the system parameters.

This paper proposes a modified self-synchronized synchronverter for unbalanced power grids and analyzes the system performance using a small signal model. The contributions of this paper are summarized as the following three aspects. (1) The small signal model for a synchronverter is established and it is observed that the stability margin around 50 Hz is very limited, especially when the control gain of reactive power increases. (2) Lowpass filters are applied to the current feeding loop to enhance the stability of the synchronverter and eliminate the power ripples at the frequency of 50 Hz. The effectiveness of the power ripple elimination method is verified by small signal analyses. (3) A resonant-based strategy is proposed to restrain the current harmonics and power ripples in unbalanced power grid. The parameters are designed according to the small signal analyses, and the effectiveness is also validated by the small signal analyses. In a word, the goal of this paper is to improve the quality of the powers and currents flowed into the grid, and make the self-synchronized process more precise under unbalanced grid condition.

The rest of this paper is organized as follows: in Section 2, the conventional self-synchronized synchronverter in a balanced power grid is introduced, and a power ripple elimination method is proposed. Small signal model analyses prove that the proposed method can enhance the system stability and reduce power ripples. In Section 3, the influence of unbalanced grid voltage on the conventional synchronverter is analyzed and a resonant-based strategy is proposed to restrain the current harmonics and power ripples in unbalanced power grid. The parameter design method of the proposed strategy is analyzed. Then in Section 4, comparative experimental studies are conducted to confirm the effectiveness of the proposed strategy in both the self-synchronized mode and power-control mode. Finally, the conclusions are presented in Section 5.

2. Self-Synchronized Synchronverter in a Balanced Power Grid and Its Power Ripple Elimination

2.1. Self-Synchronized Synchronverter

The topology of a DC/AC converter is illustrated in Figure 1. The reference point of v_a, v_b, v_c is the neutral of the grid, and the reference point of e_a, e_b, e_c is the half of DC link voltage. To mimic the characteristics of the SG, the synchronverter is proposed according to the mechanical and excitation equations of the SG. The control diagram of the conventional synchronverter in [13] is shown in Figure 2, where the physical circuit is simplified as the mathematical model. In order to simplify the small signal analyses, the control scheme of the synchronverter is based on the reference frame where the d-axis is aligned to the rotor of synchronverter, which is named as control *dq* frame in this paper.

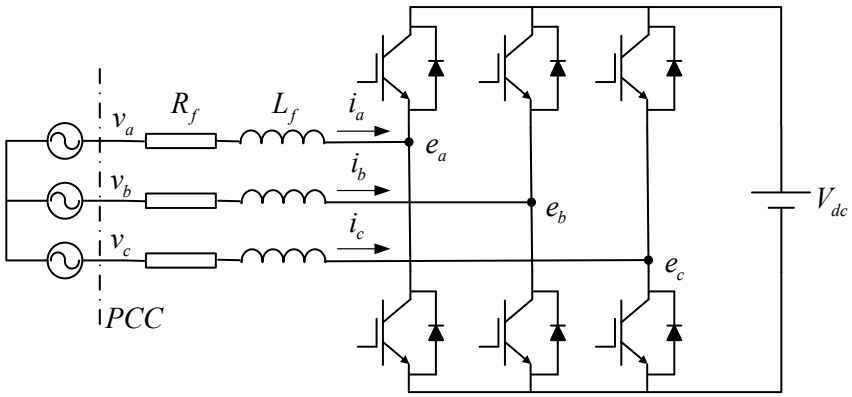

Figure 1. Topology of DC/AC converter.

The superscript r indicates that the variables are in the control dq frame. J is the moment of inertia, D is the damping factor, K is the integral factor. The phase angle θ_r of the converter voltage, also known as the back electrical magnetic field (EMF) of VSG, is produced by the active power controller. The amplitude of the converter voltage E is produced by the reactive power controller. ω_n is the rated angular frequency which is 100π (50 Hz) in this paper. The i^r_{dq} can be expressed as:

$$\begin{bmatrix} i^r_d \\ i^r_q \end{bmatrix} = \frac{2}{3}\begin{bmatrix} \cos\theta_r & \cos(\theta_r - 2\pi/3) & \cos(\theta_r + 2\pi/3) \\ -\sin\theta_r & -\sin(\theta_r - 2\pi/3) & -\sin(\theta_r + 2\pi/3) \end{bmatrix}\begin{bmatrix} i_a \\ i_b \\ i_c \end{bmatrix} \tag{1}$$

The reference voltage e^r_{dq} in the control dq frame is calculated as:

$$\begin{cases} e^r_d = 0 \\ e^r_q = -E = -\omega_r \psi_f \end{cases} \tag{2}$$

The electromagnetic active and reactive powers are calculated as:

$$\begin{cases} P_e = e_q^r i_q^r = -\omega_r \psi_f i_q^r \\ Q_e = e_q^r i_d^r = -\omega_r \psi_f i_d^r \end{cases} \tag{3}$$

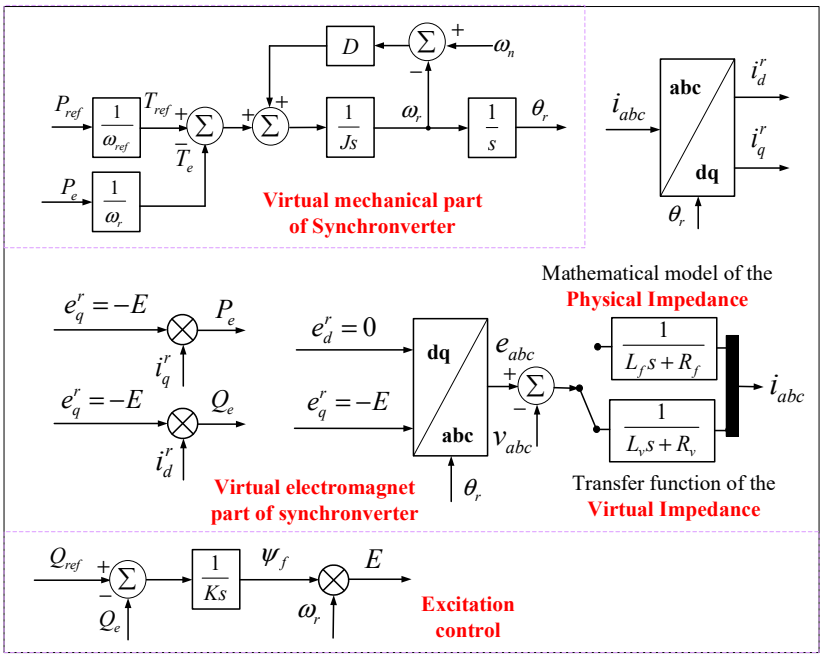

Figure 2. Control diagram of the conventional synchronverter.

To synchronize with the grid voltage without PLL, a self-synchronized method can be adopted [14]. As the grid currents are zero before the switch is closed, the control process is not effective. Therefore, virtual impedances are introduced to simulate the inductance and resistance between the converter and the grid. The virtual currents are calculated according to the grid voltages, converter voltages and virtual impedance as follows:

$$i_{vabc} = \frac{1}{L_v s + R_v}(e_{abc} - v_{abc}) \tag{4}$$

Therefore, when the virtual powers (calculated in the same way as (3)) are controlled to be zero, the virtual currents will be zero simultaneously, which means that the converter voltages have been synchronized with the grid voltages. Finally, when the connection process is finished, the real grid currents are used to replace the virtual currents to calculate the feedback powers.

2.2. Small Signal Analysis and Power Ripple Elimination

The small signal model of synchronverter is developed in synchronous reference frame aligned to the fundamental grid voltage vector [27], which is called system dq frame in this paper in order to distinguish from the control *dq* frame. In this paper, variables with superscripts *s* means they are in the system *dq* frame. Its phase angle θ_1 is calculated as:

$$\theta_1 = \omega_1 t \tag{5}$$

In the normal operation, ω_1 is equal to ω_n. The phase angle difference δ between the system *dq* frame and control *dq* frame is calculated as:

$$\delta = \theta_r - \theta_1 \tag{6}$$

The relationships between variables in the system dq frame and their counterparts in control frame are shown as:

$$\begin{aligned} x_{dq}^{s} &= \begin{bmatrix} x_d^s \\ x_q^s \end{bmatrix} = \begin{bmatrix} \cos\delta & -\sin\delta \\ \sin\delta & \cos\delta \end{bmatrix} \begin{bmatrix} x_d^r \\ x_q^r \end{bmatrix} \\ x_{dq}^{r} &= \begin{bmatrix} x_d^r \\ x_q^r \end{bmatrix} = \begin{bmatrix} \cos\delta & \sin\delta \\ -\sin\delta & \cos\delta \end{bmatrix} \begin{bmatrix} x_d^s \\ x_q^s \end{bmatrix} \end{aligned} \tag{7}$$

For the synchronverter system studied in the paper, the x in (7) includes output current i_{dq}, grid voltage v_{dq}, and converter voltage e_{dq}.

The derivative of the currents in the system dq frame can be expressed as follows:

$$\begin{cases} di_d^s/dt = (\omega_1 L_f i_q^s - R_f i_d^s + e_d^s - v_d^s)/L_f \\ di_q^s/dt = (-\omega_1 L_f i_d^s - R_f i_q^s + e_q^s - v_q^s)/L_f \end{cases} \tag{8}$$

According to Figure 2, the swing equation of synchronverter is expressed as:

$$d\omega_r/dt = [T_m - T_e - D_p(\omega_r - \omega_1)]/J \tag{9}$$

where $T_m = P_{ref}/\omega_n$, is the nominal virtual mechanical torque input of synchronverter.

The excitation model of synchronverter can be expressed as:

$$d\psi_f/dt = K(Q_{ref} - Q_e) \tag{10}$$

Combining the equations above, the nonlinear model of the synchronverter can be obtained as follows:

$$\begin{cases} di_d^s/dt = (\omega_1 L_f i_q^s - R_f i_d^s + \omega_r \psi_f \sin\delta - v_d^s)/L_f \\ di_q^s/dt = (-\omega_1 L_f i_d^s - R_f i_q^s - \omega_r \psi_f \cos\delta - v_q^s)/L_f \\ d\omega_r/dt = [T_m - T_e - D_p(\omega_r - \omega_1)]/J \\ d\delta/dt = \omega_r - \omega_1 \\ d\psi_f/dt = K(Q_{ref} - Q_e) \end{cases} \tag{11}$$

Linearizing these equations around the steady state, the small signal model can be expressed in state space form as:

$$\begin{cases} \dot{\boldsymbol{x}} = \boldsymbol{A}\boldsymbol{x} + \boldsymbol{B}\boldsymbol{u} \\ \boldsymbol{y} = \boldsymbol{C}\boldsymbol{x} + \boldsymbol{D}\boldsymbol{u} \end{cases} \tag{12}$$

where the state vector $\boldsymbol{x}$ includes the variables shown in (13):

$$\boldsymbol{x} = \left[\Delta i_d^s, \Delta i_q^s, \Delta\omega, \Delta\delta, \Delta\psi_f\right]^T \tag{13}$$

input vector $\boldsymbol{u}$ includes variables shown in (14):

$$\boldsymbol{u} = \left[\Delta v_d^s, \Delta v_q^s, \frac{\Delta P_{ref}}{\omega_n}, \Delta Q_{ref}\right]^T \tag{14}$$

and output vector $\boldsymbol{y}$ includes variables shown in (15):

$$\boldsymbol{y} = \left[\Delta i_d^s, \Delta i_q^s, \Delta T_e, \Delta Q_e\right]^T \tag{15}$$

For simplicity, the 'Δ', denoting perturbation variables, can be omitted when it comes to the linearized small signal system.

The detailed expressions of $\boldsymbol{A}$, $\boldsymbol{B}$, $\boldsymbol{C}$ and $\boldsymbol{D}$ in (12) can be calculated by Matlab, which are shown as follows:

$$\boldsymbol{A} = \begin{bmatrix} -R_f/L_f & \omega_1 & \psi_f \sin\delta/L_f & \omega_r\psi_f \cos\delta/L_f & \omega_r \sin\delta/L_f \\ -\omega_1 & -R_f/L_f & -\psi_f \cos\delta/L_f & \omega_r\psi_f \sin\delta/L_f & -\omega_r \cos\delta/L_f \\ -\psi_f \sin\delta/J & \psi_f \cos\delta/J & -D_p/J & -\psi_f(i_d^s \cos\delta + i_q^s \sin\delta)/J & (i_q^s \cos\delta + i_d^s \sin\delta)/J \\ 0 & 0 & 1 & 0 & 0 \\ K\omega_r\psi_f \cos\delta & K\omega_r\psi_f \sin\delta & K\psi_f(i_d^s \cos\delta + i_q^s \sin\delta) & K\omega_r\psi_f(i_q^s \cos\delta - i_d^s \sin\delta) & K\omega_r(i_d^s \cos\delta + i_q^s \sin\delta) \end{bmatrix}$$

$$\boldsymbol{B} = \begin{bmatrix} -1/L_s & 0 & 0 & 0 \\ 0 & -1/L_s & 0 & 0 \\ 0 & 0 & 1/J & 0 \\ 0 & 0 & 0 & 0 \\ 0 & 0 & 0 & K \end{bmatrix} \quad \boldsymbol{D} = \begin{bmatrix} 0 & 0 & 0 & 0 \\ 0 & 0 & 0 & 0 \\ 0 & 0 & 0 & 0 \\ 0 & 0 & 0 & 0 \end{bmatrix}$$

$$\boldsymbol{C} = \begin{bmatrix} 1 & 0 & 0 & 0 & 0 \\ 0 & 1 & 0 & 0 & 0 \\ \psi_f \sin\delta & -\psi_f \cos\delta & 0 & \psi_f(i_d^s \cos\delta + i_q^s \sin\delta) & i_d^s \sin\delta - i_q^s \cos\delta \\ -\omega_r\psi_f \cos\delta & -\omega_r\psi_f \sin\delta & -\psi_f(i_d^s \cos\delta + i_q^s \sin\delta) & -\omega_r\psi_f(i_q^s \cos\delta - i_d^s \sin\delta) & -\omega_r(i_d^s \cos\delta + i_q^s \sin\delta) \end{bmatrix}$$

In this study, a small scale 1000 W converter system is used to test the synchronverter control scheme. Its parameters are listed in Table 1.

Table 1. Parameters of VSG system.

System Parameters	Value
Grid voltage	130 V
Rated frequency	50 Hz
Input resistance	0.1 Ω
Input inductance	6 mH
DC bus voltage	280 V

The damping coefficient D is a pre-defined parameter according to desired active power drooping profile, e.g., when the grid frequency decreased by 0.5 Hz, the converter shall generate an additional 100% rated power to support the grid. J and K are considered as tuning parameters. Their impacts on the dynamic of synchronverter are illustrated by pole-zero maps as shown in Figures 3 and 4 using the symbol of blue cross according to (12).

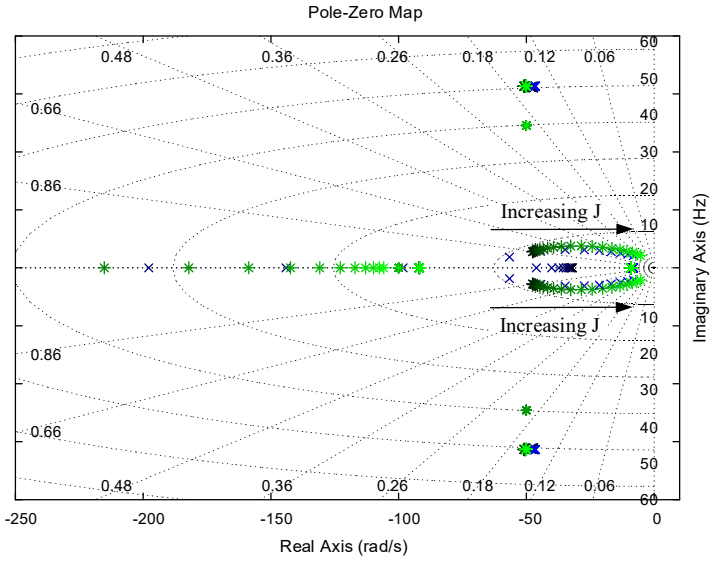

Figure 3. The impact of J (increased from 0.06 to 6) and the introduced current lowpass filters on the poles distribution of synchronverter system. Cross: poles without current lowpass filters. Asterisk: poles with current lowpass filters.

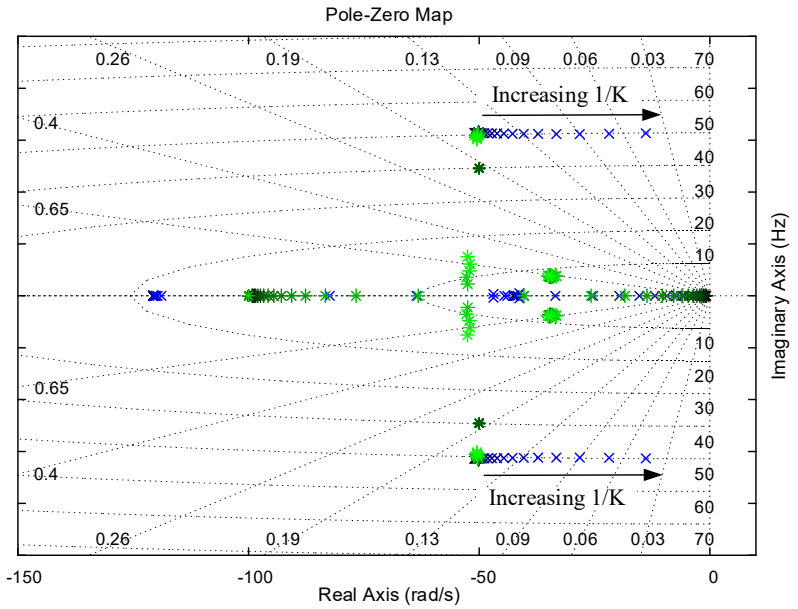

Figure 4. The impact of $1/K$ (increased from 0.075 to 7.5) and the introduced current lowpass filters on the poles distribution of synchronverter system. Cross: poles without current lowpass filters. Asterisk: poles with current lowpass filters.

It's observed in Figures 3 and 4 that with the increase of J and $1/K$, the poles are pushed to the right half of the plain. It is also observed that a pair of conjugated poles at 50 Hz are damped weakly and the situation becomes even worse when the control gain of reactive power ($1/K$) increases. Such a limited stability margin could jeopardize the stable operation of synchronverter due to insufficient noise rejection capability. Thus, there will be power ripples at the frequency of 50 Hz.

In order to eliminate the power ripples, two lowpass filters are applied to the current feeding loop in the synchronverter. The filters are designed in the control dq frame, so the frequency of filter is selected as 0 Hz. The filtered currents can be expressed as follows:

$$i^r_{fd} = \frac{1/\omega_c}{s+1/\omega_c} i^r_d \quad i^r_{fq} = \frac{1/\omega_c}{s+1/\omega_c} i^r_q \tag{16}$$

where ω_c is the cutoff frequency. The grid frequency is likely to drift in the situation where synchronverter is applied. Thus, in order to sufficiently reject noises higher than 50 Hz and leave enough margin for grid frequency drift, the cut-off frequency is chosen as 16 Hz.

Equation (16) can also be expressed as follows:

$$\begin{cases} di^r_{fd}/dt = (i^r_d - i^r_{fd})/\omega_c \\ di^r_{fq}/dt = (i^r_q - i^r_{fq})/\omega_c \end{cases} \tag{17}$$

Considering (17), the state space model in (12) is modified accordingly as:

$$\begin{cases} \dot{\boldsymbol{x}}_f = \boldsymbol{A}_f \boldsymbol{x}_f + \boldsymbol{B}_f \boldsymbol{u} \\ \boldsymbol{y} = \boldsymbol{C}_f \boldsymbol{x}_f + \boldsymbol{D}_f \boldsymbol{u} \end{cases} \tag{18}$$

where:

$$\boldsymbol{x}_f = \left[i^s_d, i^s_q, i^r_{fd}, i^r_{fq}, \omega_r, \delta, \psi_f \right]^T \tag{19}$$

The detailed expressions of $\boldsymbol{A}_f$, $\boldsymbol{B}_f$, $\boldsymbol{C}_f$ and $\boldsymbol{D}_f$ in (18) can be calculated by Matlab, which are very complicated. Therefore, they are not presented for the conciseness of the paper.

The effectiveness of the proposed lowpass filter based current feeding loops is also demonstrated in Figures 3 and 4 using the symbol of green asterisk according to (18). It can be seen that the conjugated poles of modified synchronverter at 50 Hz move to the left and are less sensitive to the increase of $1/K$.

The effectiveness of the proposed filter based power ripple elimination method is illustrated by the bode diagram of transfer function from $[v_d, v_q]^{\mathrm{T}}$ to $[P_e, Q_e]^{\mathrm{T}}$ as shown in Figure 5. It's observed that compared with the conventional strategy, the peak gain from $[v_d, v_q]^{\mathrm{T}}$ to the powers, which lies at 50 Hz, is considerably reduced by adding the lowpass filter. Therefore, the power ripples caused by the disturbance $[v_d, v_q]^{\mathrm{T}}$ will be restrained effectively. In addition, the lowpass filter has limited impact on the transfer function from reference $[P_{ref}, Q_{ref}]^{\mathrm{T}}$ to feedback $[P_e, Q_e]^{\mathrm{T}}$, which indicates that the lowpass filter has little impact on the power reference tracking of the conventional synchronverter.

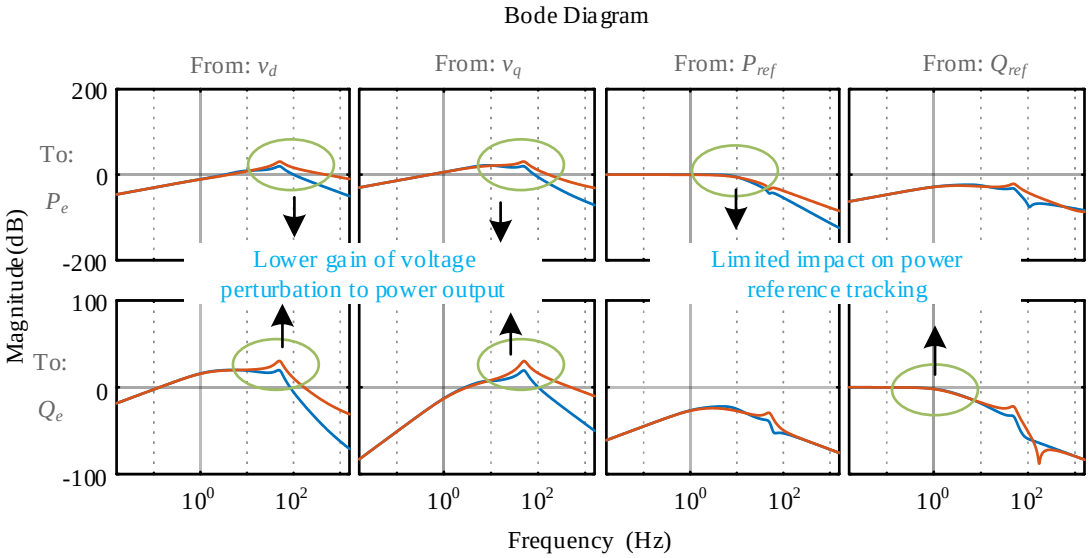

Figure 5. Bode diagram illustrating noise rejection enhancement by adding lowpass filters. Red: without lowpass filters. Blue: with lowpass filters.

3. Self-Synchronized Synchronverter in an Unbalanced Power Grid

3.1. Influence of Unbalanced Grid Voltage

The grid voltage and current have both the negative and positive sequence components when the grid voltage becomes unbalanced, which will cause double frequency ripple components in the reactive and active powers [20]. Power control of conventional synchronverter has limited bandwidth. Thus, power ripples cannot be suppressed in unbalanced power grid, which will seriously affect the control performance of the synchronverter.

In addition, the self-synchronization method proposed in [14] needs to generate a converter voltage very close to the grid voltage in order to avoid the current rushing at the moment when the converter is connected to the grid. However, when the grid voltage becomes unbalanced, the negative sequence current components (-100 Hz in synchronous reference frame) cannot be damped in the conventional synchronverter, which means that the converter voltage cannot precisely follow the grid voltage. Therefore, it's necessary to improve the conventional self-synchronized synchronverter in unbalanced power grid to restrain the negative sequence current and further guarantee the precision of the self-synchronization.

3.2. Modified Self-Synchronized Synchronverter

In the proposed modified self-synchronized synchronverter, the control scheme is expanded into a higher dimensional multiple input multiple output (MIMO) system, i.e., output currents reference $\left[i^r_{dref}, i^r_{qref}\right]^T$ are added into input vector $\boldsymbol{u}$ in (18). The output current references are set to zero.

Then, suppressing double frequency current oscillations in synchronous reference frame is equivalent to guaranteeing current reference tracking only at ±100 Hz. A SOGI based resonant controller is adopted in order to realize this purpose in this paper. The transfer function of the resonant controller is shown as:

$$H_R(s) = \frac{2k_r\omega_{cr}s}{s^2 + 2\omega_{cr}s + {\omega_s}^2} \tag{20}$$

where k_r is the gain parameter; ω_{cr} is the cutoff frequency; ω_s is the selected frequency (±100 Hz). Since the grid frequency is likely to drift in the situation where synchronverter is applied, the cutoff frequency ω_{cr} shall not be too small [27]. In this paper, ω_{cr} is chosen as 10 rad/s, so that the gain of resonant controller is reduced to 0.77 times the nominal gain when the grid frequency is drifted by 0.5 Hz from the nominal 50 Hz.

The modified control diagram is shown in Figure 6. The inputs of resonant controller are the errors between reference and feedback currents (virtual current in the self-synchronization mode, grid current in the power-control mode) and the outputs of resonant controller are added to converter voltage reference generated by power control part of synchronverter. The final converter voltage reference e^r_{fd} and e^r_{fq} can be expressed as follows:

$$\begin{cases} e^r_{fd} = e^r_{cd} + e^r_d = e^r_{cd} \\ e^r_{fq} = e^r_{cq} + e^r_q = e^r_{cq} - \omega_r\psi_f \end{cases} \tag{21}$$

where e^r_{cd} and e^r_{cq} are the outputs of the resonant controllers.

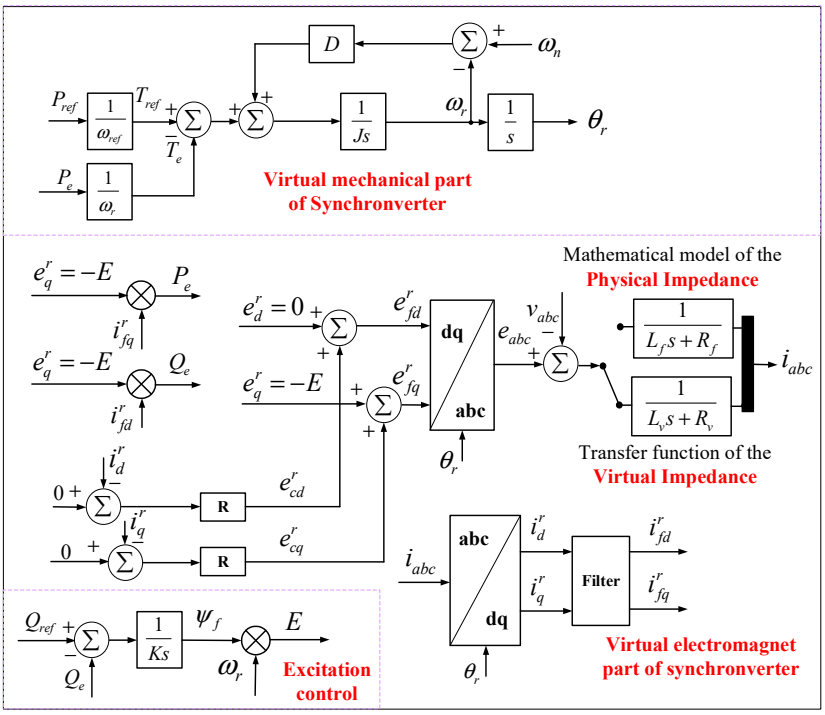

Figure 6. Control diagram of the proposed self-synchronized synchronverter in unbalanced power grid.

It should be noted that the sum of the three phase virtual currents calculated by (4) will not be zero in unbalanced power grid. Thus, the calculation process of the virtual currents is revised as (22):

$$i_{va} = \frac{e_a - v_a}{L_v s + R_v} \quad i_{vb} = \frac{e_b - v_b}{L_v s + R_v} \quad i_{vc} = -i_{va} - i_{vb} \tag{22}$$

To analyze the characteristics of the proposed strategy, the small signal model of synchronverter needs to be expanded considering two extra resonant controllers. According to (20), the following equations can be obtained:

$$\begin{cases} d^2e^r_{cd}/dt^2 + 2\omega_{cr}de^r_{cd}/dt + \omega_s^2 e^r_{cd} = -2k_r\omega_{cr}di^r_d/dt \\ d^2e^r_{cq}/dt^2 + 2\omega_{cr}de^r_{cq}/dt + \omega_s^2 e^r_{cq} = -2k_r\omega_{cr}di^r_q/dt \end{cases} \tag{23}$$

Equation (23) can also be expressed as follows:

$$\begin{cases} d\gamma_{d1}/dt = \gamma_{d2} \\ d\gamma_{d2}/dt = -2\omega_{cr}\gamma_{d2} - \omega_s^2\gamma_{d1} - 2k_r\omega_{cr}di^r_d/dt \\ d\gamma_{q1}/dt = \gamma_{q2} \\ d\gamma_{q2}/dt = -2\omega_{cr}\gamma_{q2} - \omega_s^2\gamma_{q1} - 2k_r\omega_{cr}di^r_q/dt \end{cases} \tag{24}$$

where:

$$\begin{cases} \gamma_{d1} = e^r_{cd} \\ \gamma_{d2} = de^r_{cd}/dt \\ \gamma_{q1} = e^r_{cq} \\ \gamma_{q2} = de^r_{cq}/dt \end{cases} \tag{25}$$

Considering (21) and (24), the new state space can be expressed as follows:

$$\begin{cases} \dot{\boldsymbol{x}}_r = \boldsymbol{A}_r\boldsymbol{x}_r + \boldsymbol{B}_r\boldsymbol{u} \\ \boldsymbol{y} = \boldsymbol{C}_r\boldsymbol{x}_r + \boldsymbol{D}_r\boldsymbol{u} \end{cases} \tag{26}$$

where $\boldsymbol{x}_r$ includes additional states introduced by resonant controllers, which can be shown as follows:

$$\boldsymbol{x}_r = \left[i^s_d, i^s_q, i^r_{fd}, i^r_{fq}, \omega_r, \delta, \psi_f, \gamma_{d1}, \gamma_{d2}, \gamma_{q1}, \gamma_{q2}\right]^T \tag{27}$$

The detailed expressions of $\boldsymbol{A}_r$, $\boldsymbol{B}_r$, $\boldsymbol{C}_r$ and $\boldsymbol{D}_r$ in (26) can be calculated by Matlab, which are very complicated. Therefore, they are not presented for the conciseness of the paper.

Nevertheless, it needs to be clarified that because of the unbalanced power grid, there are additional periodic components in the steady operation point. However, since the overall system shows lowpass filter characteristic and limited unbalance degree, the modelling error caused by the periodic components in steady state is acceptable [28].

The comparison of bode diagrams of both the conventional and modified synchronverter are illustrated in Figure 7 according to (12) and (26). The red line in Figure 7 is the bode diagram of conventional synchronverter and it's observed that the magnitude of transfer function from $[v_d, v_q]^{\mathrm{T}}$ to $\left[i^r_d, i^r_q\right]^T$ at 100 Hz is much higher than 0 dB. It means that the negative sequence component in unbalanced grid voltage will be amplified in the control system and finally results in large negative sequence output current. The resonant controllers enable the synchronverter to have current reference tracking capability at 100 Hz in synchronous reference frame because of the unity gain of the transfer function from $\left[i^r_{dref}, i^r_{qref}\right]^T$ to $\left[i^r_d, i^r_q\right]^T$ at 100 Hz. After adding resonant controllers, the magnitude of the transfer function from $[v_d, v_q]^{\mathrm{T}}$ to $\left[i^r_d, i^r_q\right]^T$ at 100 Hz reduces significantly. This verifies the effectiveness of proposed negative sequence current suppression strategy using a resonant controller. In addition, the magnitude of transfer function from $[v_d, v_q]^{\mathrm{T}}$ to $[P_e, Q_e]^T$ at 100 Hz also reduces significantly, which means that the double frequency power ripples can also be reduced by using resonant controller.

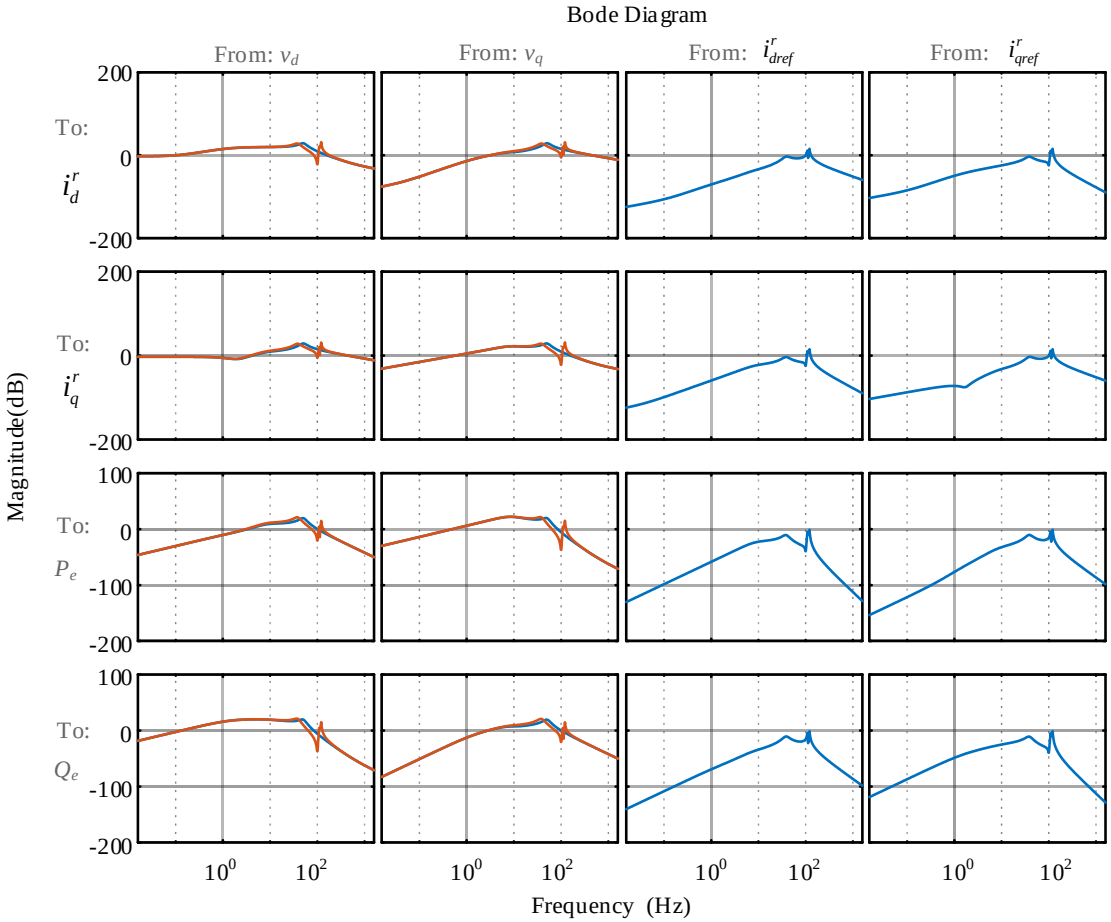

Figure 7. Bode diagram illustrating the effect of proposed resonant controller. Blue line: modified synchronverter with additional resonant controller. Red line: conventional synchronverter.

3.3. Parameter Design of The Resonant Controller

As the resonant controller has a wide resonance peak against frequency variation, the impact of resonant controller to the system stability needs to be considered, and the resonant controller gain k_r needs to be designed properly. According to the analyses of power control loop demonstrated in Section 2.2, the parameters D, J, $1/K$ are chosen as 100, 0.6, 0.75, respectively, and the bandwidth of resonant controller is chosen as 10 rad/s. In order to investigate the influence of the parameter k_r to the stability of the control system, the pole-zero map of the modified synchronverter with different k_r is shown in Figure 8 according to Equation (26). In addition, to verify the effectiveness of the proposed filter based power ripple elimination method in unbalanced power grid, the results with and without the current lowpass filters are shown as blue asterisk and green cross, respectively.

It can be observed that two additional pairs of conjugate poles are added at around 100 Hz, which are caused by resonant controllers. It can be seen from Figure 8 that the increasing k_r will drive the poles to the right, and too large k_r may push the poles related to resonant controller to the right half of the plane so that the system will become unstable. Moreover, Figure 8 also shows that the current lowpass filter can make the poles at around 50 Hz move to the left, and it has very limited impact on poles related to the resonant controller. Based on the analyses above, the control parameters for the modified synchronverter can be selected as shown in Table 2, where all the parameters are normalized values.

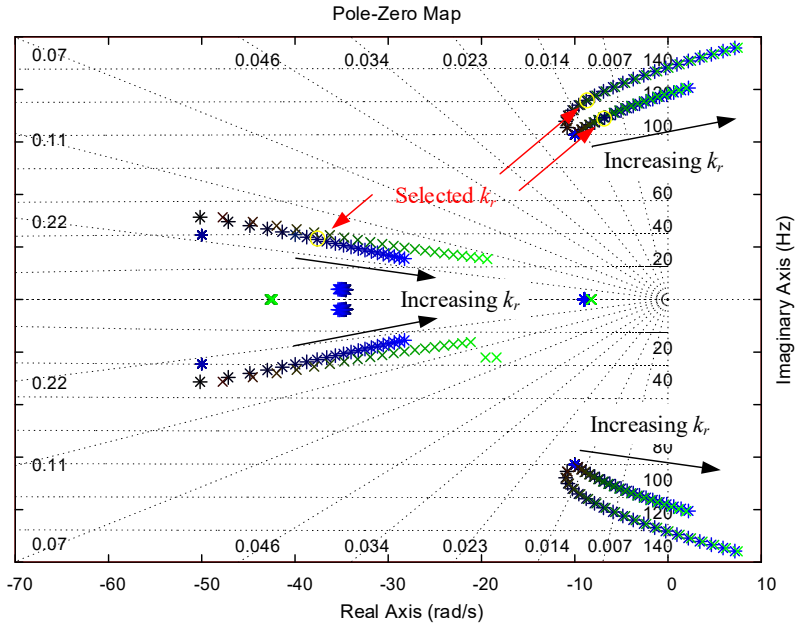

Figure 8. The impact of *kr* (increased from 0 to 6.3) and the introduced current lowpass filters on the poles distribution of synchronverter system. Cross: poles without current lowpass filters. Asterisk: poles with current lowpass filters.

Table 2. Parameters of VSG system.

System Parameters	Value
Virtual inertia J	0.6
Damping coefficient D	100
Excitation integral gain $1/K$	0.75
Gain of resonant controller k_r	1.86

4. Experimental Studies

4.1. Experimental Setup

Comparative experimental studies are conducted for the conventional and proposed synchronverters in an unbalanced power grid. The experimental platform is set up as shown in Figure 9. A TMS320F2812 Digital Signal Processor is used as the microprocessor. The unbalanced grid voltages are simulated using a transformer by making one phase of the voltages drop to 80%. The dc-bus voltage is assumed to be controlled as a constant value by the distributed generation system. Parameters of the synchronverter are shown in Tables 1 and 2. The switching frequency and sampling frequency are both set to 10 kHz. All the experimental results are shown in Figures 10–14.

4.2. Experimental Results

The dynamic responses of the conventional and proposed self-synchronized synchronverters during the grid connection process are shown in Figure 10.

Before the grid connection, the voltage errors between the grid and converter voltages are shown in α and β axes separately. And the voltage errors are changed to active and reactive powers when the switch is closed to show the dynamic response of the powers. The voltage errors contain ripples in the conventional synchronverter as shown in Figure 10a, which means that the synchronization is not precise. Thus, the currents are very large when the switch is closed. Compared with the conventional synchronverter, the voltage errors are effectively limited in the proposed synchronverter as shown in Figure 10b. In addition, the grid currents are smaller and damped much faster after the switch

is closed. Therefore, the converter can be connected to the grid more smoothly when the proposed synchronverter is used in an unbalanced power grid.

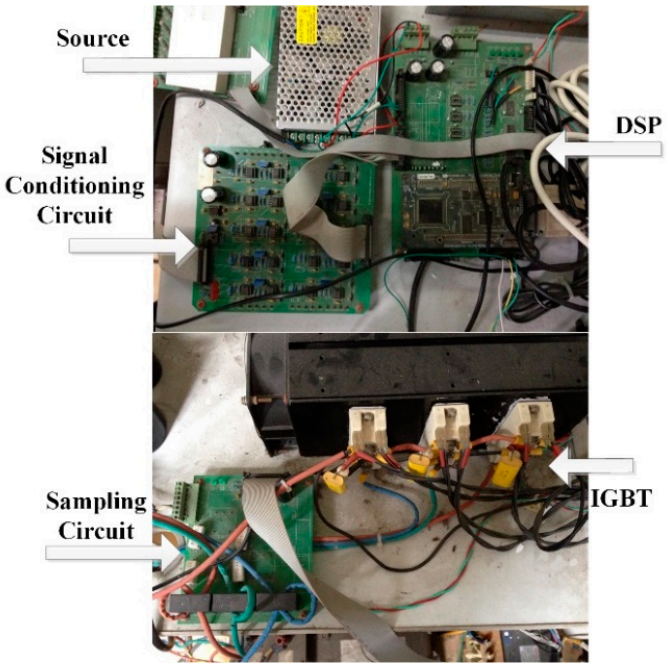

Figure 9. The experimental platform.

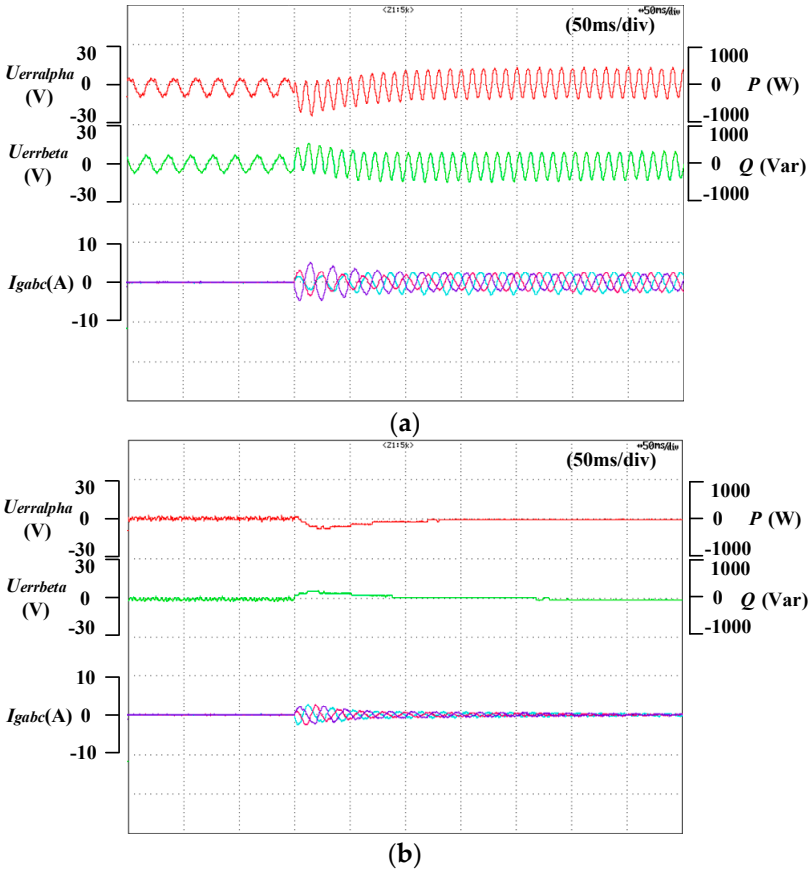

Figure 10. Dynamic responses during the grid connection process. (**a**) Conventional self-synchronized synchronverter. (**b**) Proposed self-synchronized synchronverter.

The steady-state power responses of the conventional and proposed synchronverters are shown in Figure 11. The Total Harmonic Distribution (THD) analyses of grid currents are shown in Figure 12, and the Fast Fourier Transform (FFT) analyses of active power are shown in Figure 13. In the conventional synchronverter, there are negative (−50 Hz) and third sequence (150 Hz) components in grid currents as shown in Figure 12a, and large ripples in both the reactive and active powers in Figure 11a. Current harmonics are eliminated in the proposed synchronverter as shown in Figure 12b. In addition, the power ripples are also effectively reduced in Figure 11b. Therefore, it can be concluded that the resonant based synchronverter can achieve much better control performance in unbalanced power grid compared with the conventional one.

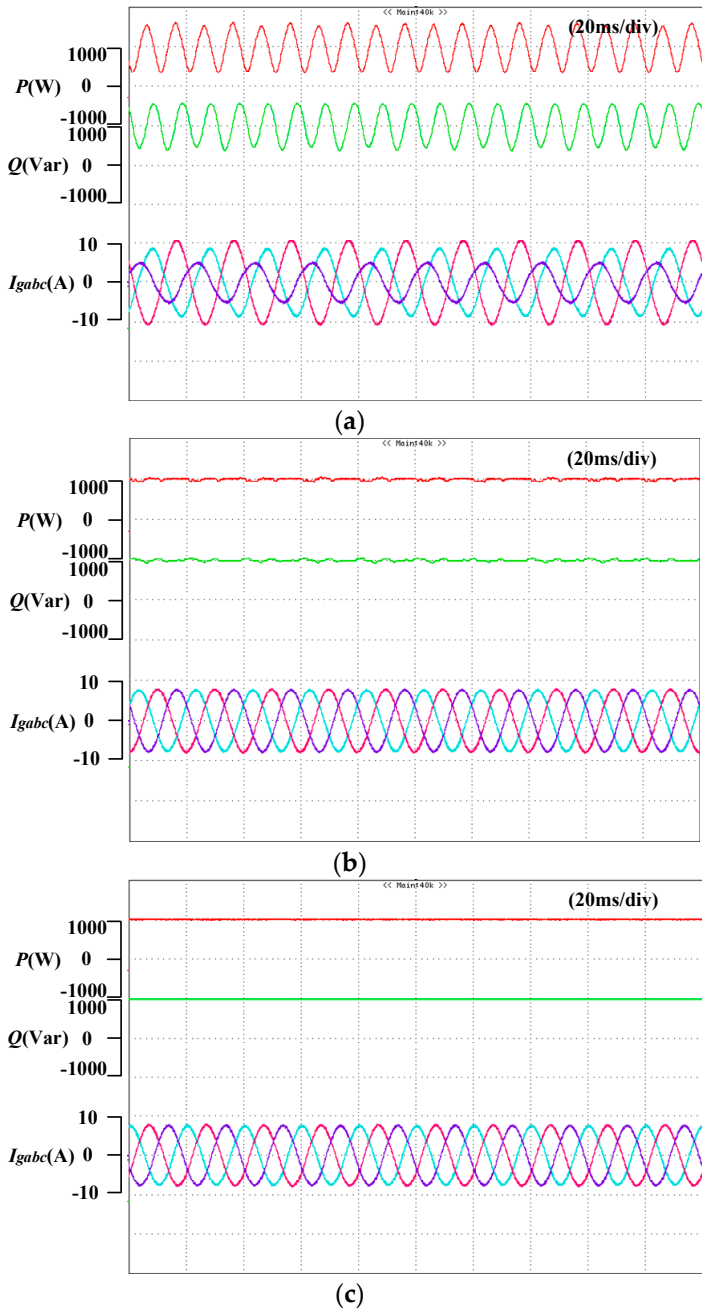

Figure 11. Steady-state responses. (**a**) Conventional synchronverter. (**b**) Proposed synchronverter without filter. (**c**) Proposed synchronverter with filter.

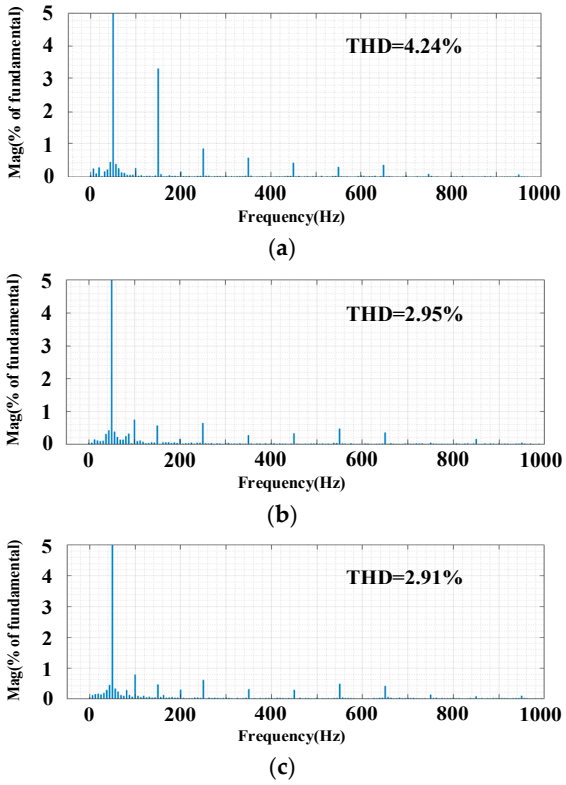

Figure 12. Grid currents THD analyses. (**a**) Conventional synchronverter. (**b**) Proposed synchronverter without filter. (**c**) Proposed synchronverter with filter.

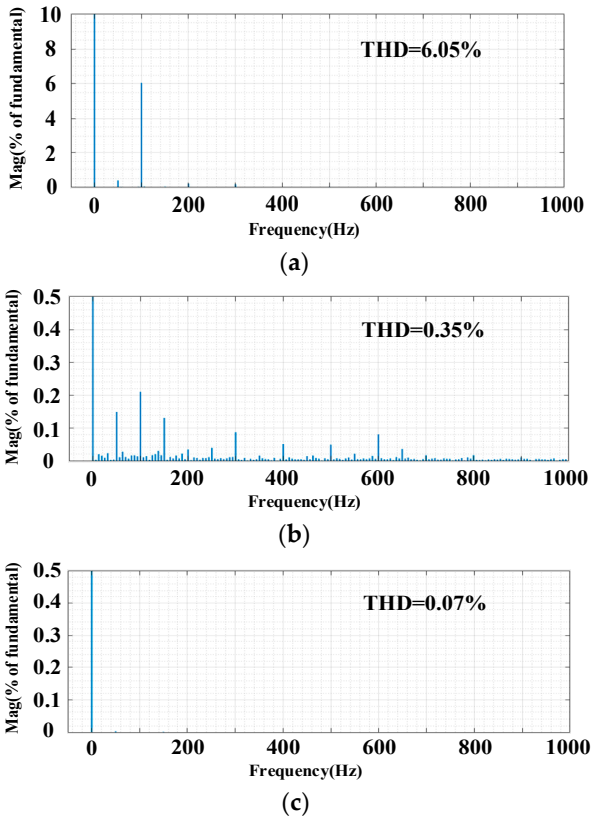

Figure 13. FFT analyses of active power. (**a**) Conventional synchronverter. (**b**) Proposed synchronverter without filter. (**c**) Proposed synchronverter with filter.

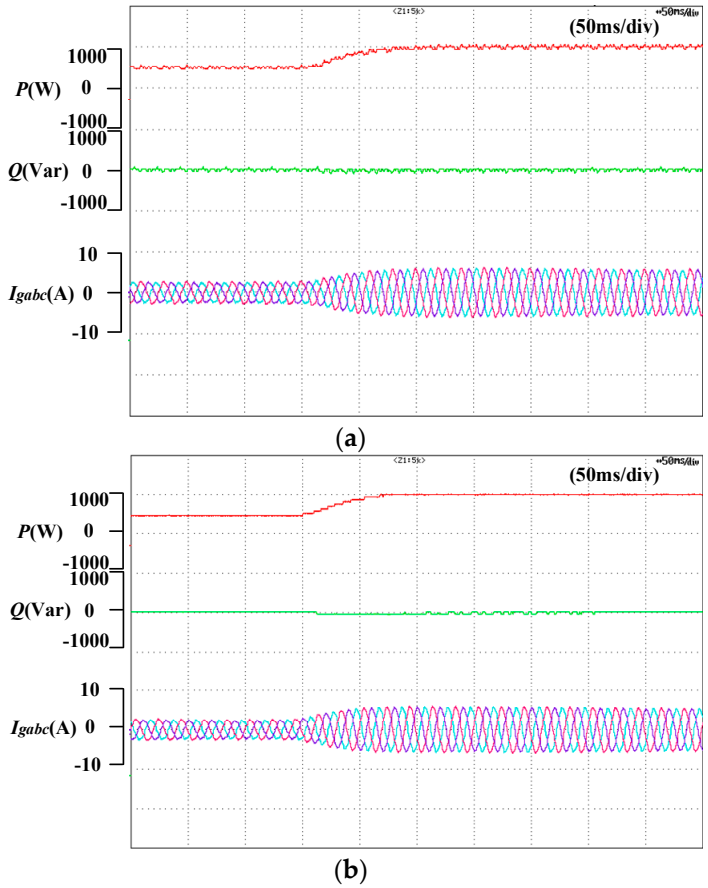

Figure 14. Active power step responses. (**a**) Proposed synchronverter without filter. (**b**) Proposed synchronverter with filter.

Compared with Figure 11b, the proposed synchronverter with filter in Figure 11c can further reduce the power ripples. It can be observed in Figure 13b that the power ripple components are mainly concentrated on the multiples of the 50 Hz, which coincides with the theoretical analyses. And the power ripples can be eliminated as shown in Figure 13c, which verifies the effectiveness of the proposed power ripple elimination method.

Besides, the impact of proposed filter on the dynamic of power control is shown in Figure 14. It's observed that the active power step responses of the proposed synchronverters without and with filter are almost identical, which verifies the analysis illustrated in Figure 5 that the filter doesn't affect the dynamic performance of the synchronverter.

5. Conclusions

A modified self-synchronized synchronverter has been proposed in this paper for unbalanced power grids. Based on the small signal analyses, it is observed that the stability margin of the conventional synchronverter around 50 Hz is very limited. Thus, a filter has been used to enhance the stability and eliminate the power ripples. In addition, a resonant-based strategy has been proposed to control the 100 Hz oscillations. Comparative experimental studies show that in the self-synchronized mode, the proposed strategy can make the synchronization more precise and the grid connection process smoother. In the power-control mode, the negative and third sequence harmonic components in grid currents can be eliminated, and the power ripples can be restrained. In addition, the power ripples can be further eliminated by the filter based method, and the dynamic control performance is not affected by the filter.

By employing the proposed strategy, the synchronverter can synchronize with the grid precisely without PLL in an unbalanced power grid, and the quality of the powers and currents flowing into the grid can be improved. Therefore, the stability of the grid can be supported by the renewable power generation systems under both balanced and unbalanced grid conditions and the efficiency of the generation systems can be increased because it does not need to disconnect from the grid under slight grid fault conditions. These merits lay the foundation for the better application of the renewable power generation in non-ideal power grid, which also lead to the great engineering practical and economic potential of the proposed strategy.

Author Contributions: Conceptualization, X.W. and D.S.; methodology, L.C. and X.W.; software, X.W. and L.C.; validation, X.W. and L.C.; formal analysis, X.W. and L.C.; data curation, D.S., L.Z. and H.N.; writing—original draft preparation, X.W. and L.C.; writing—review and editing, D.S. and H.N.; supervision, D.S. and H.N.; project administration, D.S. and L.Z.; funding acquisition, D.S. and L.Z.

Funding: This research was supported by Zhejiang Provincial Natural Science Foundation of China (No. LZ18E070001); National Natural Science Foundation of China, (No. 51622706); and Open Fund of Operation and Control of Renewable Energy & Storage Systems (China Electric Power Research Institute) (No. 1810-00893).

Conflicts of Interest: The authors declare no conflict of interest.

Nomenclature

v, e	Grid, converter voltage vectors.
i, i_v	Grid, virtual current vectors.
ψ_f	Exciting flux linkage.
P_e, Q_e	Active, reactive electromagnetic powers.
R_f, R_v	Grid, virtual resistances.
L_f, L_v	Grid, virtual inductances.
ω_1, ω_r	Synchronous, converter angular frequencies.
θ_1, θ_r	Synchronous, converter phase angles.

References

1. Huang, Y.; Zhai, X.; Hu, J.; Liu, D.; Lin, C. Modeling and Stability Analysis of VSC Internal Voltage in DC-Link Voltage Control Timescale. *IEEE J. Emerg. Sel. Top. Power Electron.* **2018**, *6*, 16–28. [CrossRef]
2. Subudhi, B.; Pradhan, R. A Comparative Study on Maximum Power Point Tracking Techniques for Photovoltaic Power Systems. *IEEE Trans. Sustain. Energy* **2013**, *4*, 89–98. [CrossRef]
3. Esram, T.; Chapman, P.L. Comparison of Photovoltaic Array Maximum Power Point Tracking Techniques. *IEEE Trans. Energy Convers.* **2007**, *22*, 439–449. [CrossRef]
4. Kundur, P.; Paserba, J.; Ajjarapu, V.; Andersson, G.; Bose, A.; Canizares, C.; Hatziargyriou, N.; Hill, D.; Stankovic, A.; Taylor, C.; et al. Definition and classification of power system stability IEEE/CIGRE joint task force on stability terms and definitions. *IEEE Trans. Power Syst.* **2004**, *19*, 1387–1401.
5. Duckwitz, D.; Fischer, B. Modeling and Design of df/dt-based Inertia Control for Power Converters. *IEEE J. Emerg. Sel. Top. Power Electron.* **2017**, *5*, 1553–1564. [CrossRef]
6. D'Arco, S.; Suul, J.A. Virtual synchronous machines-Classification of implementations and analysis of equivalence to droop controllers for microgrids. In Proceedings of the 2013 IEEE Grenoble Conference, Grenoble, France, 16–20 June 2013; pp. 1–7.
7. D'Arco, S.; Suul, J.A. Equivalence of Virtual Synchronous Machines and Frequency-Droops for Converter-Based MicroGrids. *IEEE Trans. Smart Grid* **2014**, *5*, 394–395. [CrossRef]
8. Sakimoto, K.; Miura, Y.; Ise, T. Stabilization of a power system with a distributed generator by a Virtual Synchronous Generator function. In Proceedings of the 8th International Conference on Power Electronics-ECCE Asia, Jeju, South Korea, 30 May–3 June 2011; pp. 1498–1505.
9. Wu, H.; Ruan, X.; Yang, D.; Chen, X.; Zhao, W.; Lv, Z.; Zhong, Q. Small-Signal Modeling and Parameters Design for Virtual Synchronous Generators. *IEEE Trans. Ind. Electron.* **2016**, *63*, 4292–4303. [CrossRef]

10. Liu, J.; Miura, Y.; Ise, T. Comparison of Dynamic Characteristics Between Virtual Synchronous Generator and Droop Control in Inverter-Based Distributed Generators. *IEEE Trans. Power Electron.* **2016**, *31*, 3600–3611. [CrossRef]
11. D'Arco, S.; Suul, J.A.; Fosso, O.B. Control system tuning and stability analysis of Virtual Synchronous Machines. In Proceedings of the 2013 IEEE Energy Conversion Congress and Exposition, 15–19 September 2013; pp. 2664–2671.
12. Amin, M.R.; Aizam Zulkifli, S. A framework for selection of grid-inverter synchronisation unit: Harmonics, phase-angle and frequency. *Renew. Sustain. Energy Rev.* **2017**, *78*, 210–219. [CrossRef]
13. Zhong, Q.C.; Weiss, G. Synchronverters: Inverters That Mimic Synchronous Generators. *IEEE Trans. Ind. Electron.* **2011**, *58*, 1259–1267. [CrossRef]
14. Zhong, Q.C.; Nguyen, P.L.; Ma, Z.; Sheng, W. Self-Synchronized Synchronverters: Inverters without a Dedicated Synchronization Unit. *IEEE Trans. Power Electron.* **2014**, *29*, 617–630. [CrossRef]
15. Natarajan, V.; Weiss, G. Almost global asymptotic stability of a grid-connected synchronous generator. *arXiv* **2016**; arXiv:161004858.
16. Yazdani, A.; Iravani, R. A unified dynamic model and control for the voltage-sourced converter under unbalanced grid conditions. *IEEE Trans. Power Deliv.* **2006**, *21*, 1620–1629. [CrossRef]
17. Hu, Y.; Zhu, Z.Q.; Odavic, M. Instantaneous Power Control for Suppressing the Second Harmonic DC Bus Voltage under Generic Unbalanced Operating Conditions. *IEEE Trans. Power Electron.* **2017**, *32*, 3998–4006. [CrossRef]
18. Nian, H.; Cheng, P.; Zhu, Z.Q. Independent Operation of DFIG-Based WECS Using Resonant Feedback Compensators under Unbalanced Grid Voltage Conditions. *IEEE Trans. Power Electron.* **2015**, *30*, 3650–3661. [CrossRef]
19. Cheng, P.; Nian, H. Collaborative Control of DFIG System during Network Unbalance Using Reduced-Order Generalized Integrators. *IEEE Trans. Energy Convers.* **2015**, *30*, 453–464. [CrossRef]
20. Cheng, P.; Nian, H. Direct power control of voltage source inverter in a virtual synchronous reference frame during frequency variation and network unbalance. *IET Power Electron.* **2016**, *9*, 502–511. [CrossRef]
21. Natarajan, V.; Weiss, G. Synchronverters with better stability due to virtual inductors, virtual capacitors and anti-windup. *IEEE Trans. Ind. Electron.* **2017**, *64*, 5994–6004. [CrossRef]
22. Zhong, Q.C.; Konstantopoulos, G.C.; Ren, B.; Krstic, M. Improved Synchronverters with Bounded Frequency and Voltage for Smart Grid Integration. *IEEE Trans. Smart Grid* **2018**, *9*, 786–796. [CrossRef]
23. Wu, W.; Zhou, L.; Chen, Y.; Luo, A.; Dong, Y.; Zhou, X.; Xu, Q.; Yang, L.; Guerrero, J.M. Sequence-Impedance-Based Stability Comparison between VSGs and Traditional Grid-Connected Inverters. *IEEE Trans. Power Electron.* **2019**, *34*, 46–52. [CrossRef]
24. Rodríguez-Cabero, A.; Roldan-Perez, J.; Prodanovic, M. Synchronverter small-signal modelling and eigenvalue analysis for battery systems integration. In Proceedings of the 2017 IEEE 6th International Conference on Renewable Energy Research and Applications, San Diego, CA, USA, 5–8 November 2017; pp. 780–784.
25. Dong, S.; Chen, Y.C. A Method to Directly Compute Synchronverter Parameters for Desired Dynamic Response. *IEEE Trans. Energy Convers.* **2018**, *33*, 814–825. [CrossRef]
26. Dong, S.; Chen, Y.C. Adjusting Synchronverter Dynamic Response Speed via Damping Correction Loop. *IEEE Trans. Energy Convers.* **2017**, *32*, 608–619. [CrossRef]
27. Wen, B.; Boroyevich, D.; Burgos, R.; Mattavelli, P.; Shen, Z. Analysis of D-Q Small-Signal Impedance of Grid-Tied Inverters. *IEEE Trans. Power Electron.* **2016**, *31*, 675–687. [CrossRef]
28. Gelb, A.; Vander Velde, W.E. *Multiple-Input Describing Functions and Nonlinear System Design*; McGraw-Hill: New York, NY, USA, 1968.